11 Superconductivity and Magnetism

H. Keller, J. Hofer (until June 2000), R. Khasanov, M. Mali, P. Morf,
R. Pircher (since March 2001), R. Renggli, J. Roos, A. Schilling, Ph. Schneider (since January 2001), A. Shengelaya, G.M. Zhao, S. Zech-Döttinger (until July 2000),
V.A. Ivanshin (visiting scientist),
T. Schneider (Titularprofessor), and K.A. Müller (Honorarprofessor)

in collaboration with:
ETH Zürich (J. Karpinski), Paul Scherrer Institute (E. Morenzoni, K. Conder, A. Furrer), IBM Rüschlikon Research Laboratory (C. Rossel), Max Planck Institut für Festkörperforschung, Stuttgart (H.-U. Habermeier), University of Birmingham (E.M. Forgan), University of St. Andrews (S.L. Lee), Loughborough University (A. S. Alexandrov), University of Oxford (S.J. Blundell), Rutherford Appleton Laboratory (F.L. Pratt), Institut Max von Laue-Paul Langevin, Grenoble (R. Cubitt), Kazan State University (M.V. Eremin, A.V. Dooglav, B.I. Kochelaev), University of Belgrade (I.M. Savić), Institute of Low Temperature and Structure Research, Polish Academy of Sciences, Wroclaw (P.W. Klamut), University of Maryland (R. L. Greene), Argonne National Laboratory (G.W. Crabtree), Northern Illinois University, DeKalb (B. Dabrowski), University of Houston (C. W. Chu), NEC Research Institute, Princeton (S. Bhattacharya).

11.1 Introduction

In the previous year we have continued and extended our studies of the fundamental physical properties of high-temperature superconductors (HTS) and related magnetic systems. One main research project involves detailed oxygen isotope ($^{16}O/^{18}O$) effect (OIE) studies on various physical quantities and phenomena (critical temperature, in-plane penetration depth, resistivity, charge and spin dynamics, stripe formation) in these systems in order to explore the role of lattice effects in cuprate systems. In another project, we have continued our investigation of the magnetic, electronic and thermal properties of HTS, that we have started several years ago. A great advantage of our work is the application of complementary experimental techniques, such as muon-spin rotation (μSR), nuclear magnetic resonance (NMR), nuclear quadrupole resonance (NQR,) electron paramagnetic resonance (EPR), together with bulk SQUID and torque magnetometry measurements, resistivity, and thermal measurements. The scientific merit of this work is to gain new information on the relevant physical properties of HTS and related systems which may help to clarify the nature of high-temperature superconductivity.

11.2 Studies of oxygen isotope effects

11.2.1 Oxygen isotope effects in manganites

Despite tremendous experimental efforts [1], the basic physics and the microscopic mechanism for the colossal magnetoresistance (CMR) in doped manganites remain controversial [2, 3, 4]. Several theoretical investigations [2, 3] indicate that in the paramagnetic state the electron-phonon coupling constant λ is large enough to form small polarons while the growing ferromagnetic order increases the bandwidth and thus decreases λ sufficiently to form a large polaron metallic state. On the other hand, Alexandrov and Bratkovsky [4] have recently argued that the model suggested by Millis *et al.* [2] cannot quantitatively explain CMR, and thus proposed an alternative CMR theory. The basic idea of their model is that the small polarons form localized bound pairs (bipolarons) in the paramagnetic state, while

the competing exchange interaction of the polaronic carriers with localized spins drives the ferromagnetic transition. The transition is accompanied by a giant increase in the number of small polarons which are mobile carriers and move coherently at low temperatures. This model appears to be able to explain the CMR quantitatively.

In order to discriminate among those different models, we study the oxygen ^{16}O vs. ^{18}O isotope effects on the transport properties in several doped manganites. The OIE on the intrinsic resistivity was obtained from high-quality epitaxial thin films of $La_{0.75}Ca_{0.25}MnO_3$ and $Nd_{0.7}Sr_{0.3}MnO_3$. The OIE on the thermoelectric power S was studied in ceramic samples of $La_{1-x}Ca_xMnO_3$, since the grain-boundary effect on S is negligible.

In the low-temperature ferromagnetic state, the intrinsic resistivity of these compounds shows a strong dependence on the oxygen isotope mass. The residual resistivity of the films increases by 15(3)% upon replacing ^{16}O with ^{18}O [5]. In contrast, the thermoelectric power is nearly independent of the oxygen isotope mass [6]. The observed large isotope effect on the resistivity and negligible effect on the thermoelectric power are in quantitative agreement with a theory based on a novel polaronic Fermi liquid [6]. The existence of a polaronic Fermi-liquid state in the ferromagnetic state is also consistent with the CMR theory by Alexandrov and Bratkovsky [4].

In the paramagnetic state, the resistivity data can be well fit by [7]

$$\rho = \frac{A}{\sqrt{T}} \exp(E_\rho / k_B T),$$

where $A = (ah/e^2\sqrt{k_B})(1.05W_p)^{1.5}/\hbar\omega_o$, W_p is the polaron bandwidth, and E_ρ is the activation energy. We found that, upon replacing ^{16}O with ^{18}O, the parameter A decreases by 35(5)%, and E_ρ increases by 13.2(5) meV [7]. The strong isotope dependence of E_ρ is not consistent with a simple small polaron hopping conduction mechanism where E_ρ is nearly independent of the isotope mass. However, this isotope effect is in quantitative agreement with a scenario where immobile bipolarons are formed in the paramagnetic state [7], and thus give a strong support to the CMR theory proposed by Alexandrov and Bratkovsky [4].

11.2.2 Oxygen isotope effects in cuprates

a) Charge and spin dynamics in $YBa_2Cu_4O_8$ studied by NMR/NQR

Recently we performed high accuracy ^{63}Cu NQR spin-lattice relaxation and SQUID magnetization measurements on ^{16}O and ^{18}O exchanged $YBa_2Cu_4O_8$ and determined the isotope shift of the opening of the spin-pseudogap, T^*, and the superconducting transition temperature T_c. The corresponding isotope exponents are $\alpha_{T^*} = 0.061(8)$ and $\alpha_{T_c} = 0.056(12)$, which are the same within error bars and suggest a common origin for the superconducting and the spin-pseudogap [8]. This result is in contrast to a recent study [9] which reported the absence of an OIE in the pseudogap of $YBa_2Cu_4O_8$ as determined by ^{89}Y Knight shift. To resolve this controversy we decided to perform high precision Cu Knight shift measurements on the same samples we used in the spin-lattice relaxation measurements. For this purpose we first had to measure accurately on both oxygen exchanged samples the Cu NQR frequency (zero magnetic field), shown in the left part of Fig. 11.8. After orientating the $YBa_2Cu_4O_8$ powder grains in the 9T-magnet and fixing them in epoxy resin, we performed Cu Knight shift measurements for the orientation of the grains with their c-axis perpendicular to the magnetic field. In the right part of Fig. 11.8 we exhibit the final result obtained for the Knight shift after correcting for quadrupolar effects. There is definitely an OIE on the pseudogap determined by the Cu Knight shift. For the corresponding pseudogap energy scale we find values of 239.5 K and 237.4 K for ^{16}O and ^{18}O, respectively. The Knight shift

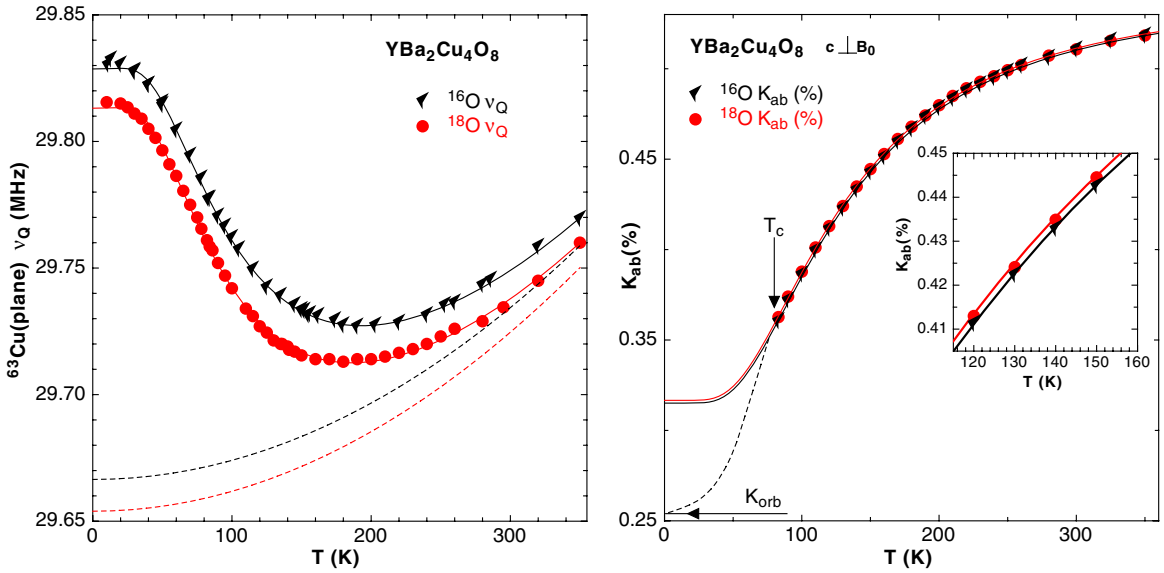

Figure 11.8: *Oxygen isotope effect on NMR and NQR of plane copper in* $YBa_2Cu_4O_8$ *. Left: temperature dependence of the NQR frequency. Right: temperature dependence of the Knight shift.*

isotope exponent amounts to 0.085(44) which is in error bar limits the same as for T^*. Thus we clearly demonstrate that spin-lattice relaxation and Knight shift show the same OIE on the pseudogap with an isotope exponent equal to the one of T_c. Looking closer at the NQR frequency (ν_Q) dependence of ^{16}O and ^{18}O samples (Fig. 11.8) we noticed an additional interesting OIE. Besides the roughly constant 15 kHz shift between the two samples which comes from the difference in the quantum mechanical zero-point displacement and thermal lattice expansion, we observed a strong OIE in the temperatures where the $\nu_Q(T)$ curves have their minima and their largest slopes, respectively. Subtracting from $\nu_Q(T)$ a lattice contribution, corrected for thermal expansion, we end up with a "rest" contribution that has to come from charge redistribution in the CuO_2 plane, presumably connected to the formation of a new pseudogap. Quantifying this "rest" contribution by fitting it with an expression similar to the one used for the Knight shift leads to energy scales of 186.4 K and 177.8 K for ^{16}O and ^{18}O, respectively. The corresponding isotope exponent was found to be 0.45(11) which is quite different from what the spin-pseudogap shows. The NQR frequency involves no spin but charge only, however, all the charges irrespective of what state they occupy. This contrasts the spin-pseudogap as observed by spin lattice-relaxation and by Knight shift where only spins of electrons close to the Fermi surface get involved. However, it is evident from the results shown in Fig. 11.8 that the NQR frequency reveals independent electronic charge features that appear to coexist with the spin-pseudogap and superconductivity.

b) Rare earth ion size effects in LaSrCuO compounds

The OIE on the suppression of the superconducting transition temperature T_c induced by the substitution of La by Eu in the compound $(La_{1-y}Eu_y)_{2-x}Sr_xCuO_4$ was systematically investigated in the framework of a diploma thesis. For this purpose, a series of samples of $(La_{1-y}Eu_y)_{2-x}Sr_xCuO_4$ with Sr contents $x = 0.1$, 0.15, and 0.20 and Eu contents $y = 0.00$, 0.05, and 0.10, were synthesized by means of standard solid state reaction sample preparation techniques. The oxygen-isotope exchange $^{16}O \rightarrow {}^{18}O$ was carried out by Dr.

K. Conder at the Paul Scherrer Institute (PSI) in Villigen, Switzerland. The superconducting

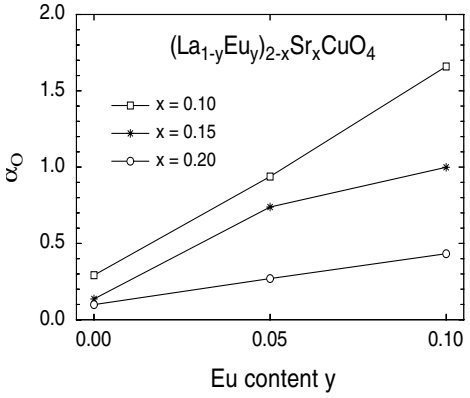

Figure 11.9: *Oxygen-isotope exponent α_O of T_c as a function of Eu substitution level in $(La_{1-y}Eu_y)_{2-x}Sr_xCuO_4$ for Sr concentrations $x = 0.10$, 0.15, and 0.20. Note that the rate at which α_O increases for the overdoped ($x = 0.20$) samples amounts only ≈27% of the rate found in the underdoped ($x = 0.10$) samples, demonstrating the strong doping dependence of the Eu induced enhancement of α_O.*

transition temperature T_c and hence its dependence on the Sr and Eu content were determined by magnetic susceptibility measurements. The results are as follows: First, T_c decreases drastically with increasing Eu concentration, whereby the T_c suppression is most efficient in the underdoped regime. Replacement of 10% of La^{3+} (ionic radius $r_K = 114$ pm) by the smaller rare-earth ion Eu^{3+} ($r_K = 95$ pm) reduces T_c below 5 K. Second, the oxygen-isotope exponent α_O of T_c decreases almost linearly with increasing charge carrier concentration, i.e. the OIE is most pronounced in the underdoped regime for all Eu concentrations. Furthermore, α_O increases nearly linearly with increasing Eu content for all charge carrier concentrations (Fig. 11.9). These findings confirm the well known generic trend that α_O is largest for lowest T_c.

Moreover, our results for the Eu induced suppression of T_c are consistent with the physical model, recently proposed for the Nd induced suppression of T_c in $(La_{1-y}Nd_y)_{2-x}Sr_xCuO_4$ [10]. The basic idea of this model involves the buckling of the CuO_2 conduction layers caused by the mismatch between the radii of the rare-earth ions which is responsible for the disappearance of superconductivity in the low temperature tetragonal (LTT) structural phase.

c) Stripe formation and structural phase transitions in LaSrCuO compounds

The observation of alternating spin and charge stripes below a characteristic temperature T^* [11, 12] has added a new feature to the phase diagram of the high-temperature cuprate superconductors. The stripe phase was suggested to be important to the understanding of the pairing mechanism in these materials [13]. However, the microscopic origin of the stripe phase is still a matter of debate. Concerning the high-T_c materials, most studies of the stripe phase were concentrated on 214 compounds with a doping level close to 1/8. It was shown that in Nd-substituted $La_{1.48}Nd_{0.4}Sr_{0.12}CuO_4$, the stripe phase is static, and no superconductivity is observed [11]. On the other hand, the stripe phase in Nd-free samples (e.g., $La_{1.94}Sr_{0.06}CuO_4$) is dynamic and superconductivity survives [14]. This indicates that Nd substitution has substantial effects on both the dynamics of the stripe phase and superconductivity.

However, it is still not clear how Nd substitution effects the physical properties of the $La_{2-x}Sr_xCuO_4$ system. The complication is associated with the fact that a partial substitution of La by Nd in $La_{2-x}Sr_xCuO_4$ induces a structural-phase transition, which occurs (for 40% substitution) at about 80 K, while the charge stripe formation takes place near 65 K. This complication is even more pronounced in the compound $La_{1.875}Ba_{0.125}CuO_4$, where the structural phase transition is clearly observable at 57 K (see Annual Report 1999/2000), while the charge stripe formation temperature is near 54 K, which renders the two transi-

tions almost indistinguishable. Therefore, it is natural to ask whether these two phenomena are related to each other. If they are related, the OIE on the charge-stripe formation temperature might be caused by the OIE on the structural phase transition temperature or vice versa. In order to clarify the situation, it is necessary to synthesize a compound in which the two transitions occur at clearly distinct temperatures. This condition is fulfilled in the compound $(La_{0.9}Eu_{0.1})_{1.875}Sr_{0.125}CuO_4$, where the structural phase transition takes place around 120 K, whereby the charge ordering temperature is 65 K [15]. Therefore, the compounds $(La_{0.9}Eu_{0.1})_{1.875}Sr_{0.125}CuO_4$ containing the oxygen isotopes ^{16}O and ^{18}O were chosen for our studies of the relation between the OIE on the charge stripe formation and the structural-phase transition temperatures.

One of the strongest signatures of a possible stripe formation in the $La_{2-x}Sr_xCuO_4$ system was found in the so-called *wipeout effect* for the ^{63}Cu NQR signal [15]. On cooling the number of ^{63}Cu nuclei contributing to the signal starts to decrease at a certain temperature (even above T_c), which is identified as the onset temperature for stripe formation. At low temperature the signal completely disappears. We performed an OIE study of the ^{63}Cu-NQR-wipeout effect in $La_{1.875}Ba_{0.125}CuO_4$ and $(La_{0.9}Eu_{0.1})_{1.875}Sr_{0.125}CuO_4$. The results are shown in Fig. 11.10. The wipeout effect is described by a normalized factor F which

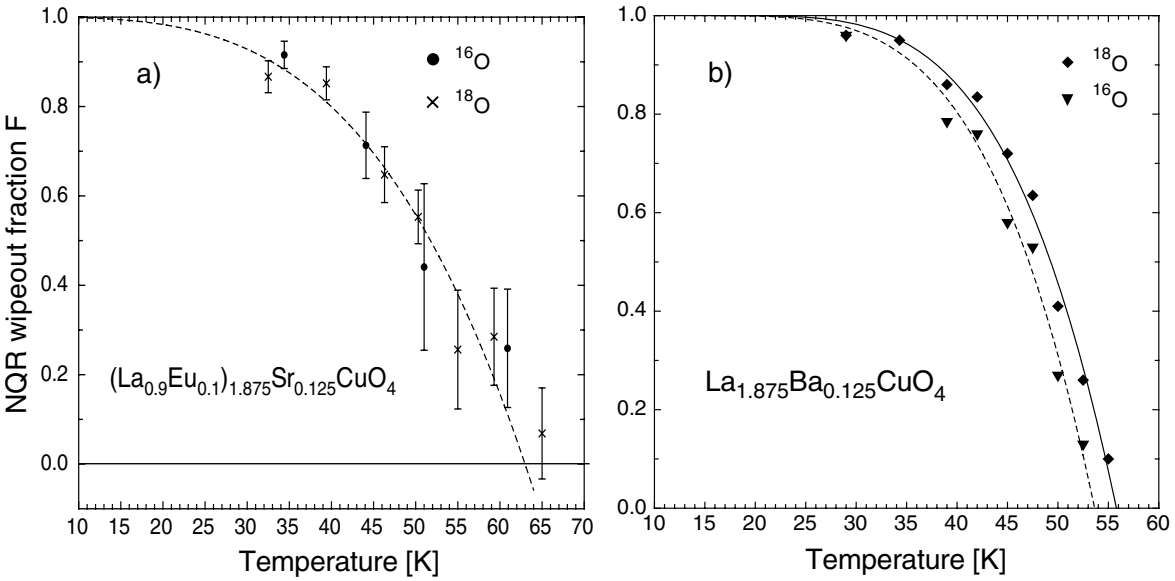

Figure 11.10: *NQR-wipeout effect in $La_{1.875}Ba_{0.125}CuO_4$ and $(La_{0.9}Eu_{0.1})_{1.875}Sr_{0.125}CuO_4$. The effect is represented by a normalized factor F, as introduced in Ref. [15]. Curves are guides to the eye.*

represents sort of an order parameter for charge stripe formation. The charge stripe formation onset-temperature in $(La_{0.9}Eu_{0.1})_{1.875}Sr_{0.125}CuO_4$ was found to be 63(2) K, which is in good agreement with the value reported in Ref. [15]. Heat capacity measurements on the identical sample revealed a clearly discernible structural phase transition at 116(2) K, in agreement with 119 K reported in earlier work [16]. However, within experimental errors we have not been able to detect any clear OIE on both transition temperatures.

This is in contrast to the situation in $La_{1.875}Ba_{0.125}CuO_4$, where we observe an oxygen-isotope shift of 2 K on both the structural phase transition around 57 K (from our heat capacity data) and on the charge stripe formation temperature (from our NQR wipeout data in Fig. 11.10b). Hence, the situation in $(La_{0.9}Eu_{0.1})_{1.85}Sr_{0.15}CuO_4$ is less clear, and we cannot

draw any further conclusions on the microscopic mechanism responsible for the occurrence of the observed phase transition and its dependence on oxygen-isotope exchange.
At this point it should be mentioned that there exists an alternative point of view concerning the interpretation of the NQR-wipeout effect as a measure of stripe order. According to Ref. [17] this effect also could be explained by the glassy nature of the magnetic freezing: slow spin dynamics shorten copper nuclear relaxation times, and these nuclei become unobservable below a threshold value of relaxation times. Because the dynamics is spatially inhomogeneous and the freezing occurs on a wide temperature interval, the NQR signal disappears gradually on cooling.

d) Measurements of the magnetic penetration depth by μSR

There is increasing evidence that a strong electron-phonon coupling is present in cuprate superconductors, which may lead to the formation of polarons (bare charge carriers accompanied by local lattice distortions) [18, 19]. However, it is not clear whether these normal-state polaronic carriers condense into Cooper pairs in the superconducting state. One way to test this hypothesis is to demonstrate that the effective mass of the supercarriers m^* depends on the mass M of the lattice atoms. This is in contrast to conventional BCS superconductors, where only the 'bare' charge carriers condense into Cooper pairs, and m^* is essentially independent of M.

According to the London model the in-plane penetration depth λ_{ab} in cuprate superconductors (clean limit) obeys the simple relation: $\lambda_{ab}^{-2}(0) \propto n_s/m_{ab}^*$, where n_s is the charge carrier density, and m_{ab}^* is the in-plane effective mass of the superconducting charge carriers. Thus a possible mass dependence of m_{ab}^* can be measured by investigating the isotope effect on the penetration depth. Previous OIE studies of the penetration depth in $La_{2-x}Sr_xCuO_4$ indeed showed a pronounced oxygen-mass dependence on the supercarrier mass [20, 21, 22]. However, in all these experiments λ was extracted indirectly, either from the Meissner fraction [20, 21], or from magnetic torque measurements [22].

The μSR technique is one of the most direct and accurate methods to determine the penetration depth λ in type II superconductors. Detailed μSR investigations of polycrystalline samples of cuprate superconductors have demonstrated that λ can be obtained from the muon spin depolarization rate $\sigma(T) \propto 1/\lambda^2(T)$, which probes the magnetic field distribution in the mixed state. For highly anisotropic superconductors (like the cuprate superconductors) λ is solely determined by the shortest penetration depth λ_{ab}, and the following relation holds [23]:

$$\sigma(T) \propto 1/\lambda_{ab}^2(T) \propto n_s/m_{ab}^*.$$

In the last year we used transverse-field μSR in order to study the OIE on λ_{ab} in underdoped powder samples of $Y_{1-x}Pr_xBa_2Cu_3O_{7-\delta}$ with $x = 0.3$ and 0.4. Preliminary results clearly indicate a pronounced OIE on λ_{ab}^{-2} which increases with decreasing T_c. For $x = 0.3$ and 0.4 the OIE was found to be $\Delta\sigma/\sigma = \Delta\lambda_{ab}^{-2}/\lambda_{ab}^{-2} = -4(1)\%$ and -7(1)%, respectively, in agreement with the recent magnetic torque measurements on $La_{2-x}Sr_xCuO_4$ [22]. These experiments are the first direct demonstration of an OIE on the magnetic penetration depth in a cuprate superconductor, implying that lattice vibrations indeed play a role in high-temperature superconductivity.

11.3 Thermal and transport studies

11.3.1 New developments in instrumentation

An old and very sensitive method to detect phase transitions in solids is the differential-thermal analysis (DTA). It is widely used in chemical sciences for measurements above room temperature. However, recently it has also been used to measure heat capacities of superconductors between 40 K and 300 K [24]. The method is so sensitive that the latent heat of vortex-lattice melting in $YBa_2Cu_3O_{7-\delta}$ could be measured for the first time [25]. We

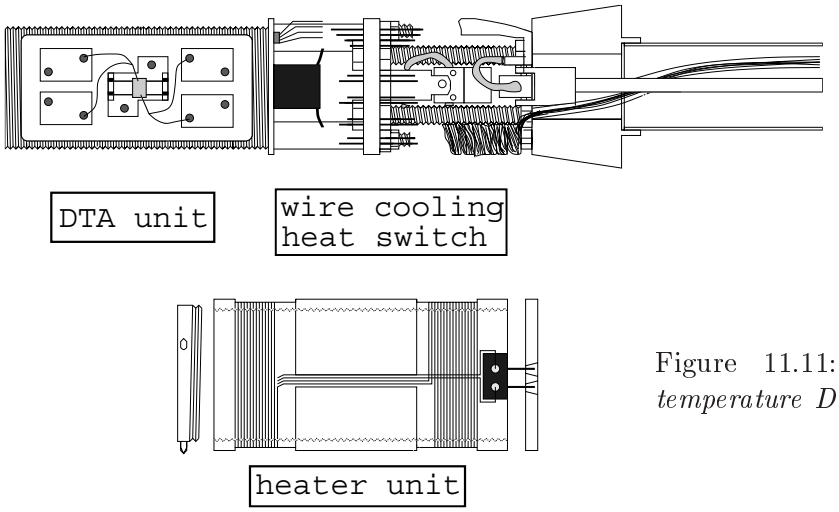

Figure 11.11: *Central part of low-temperature DTA-insert*

extended the DTA method described in Ref. [24] using cryogenic resistance thermometers. With this new setup we achieved a relative accuracy in heat capacity of at least 1 part in 10000 on samples with a mass of typically 20 mg, with a data-point density of 1000 points per Kelvin and higher. The measuring cell, shown in Fig. 11.11, is inserted into a split-coil magnet system that allows us to explore angular dependent properties in an external magnetic field. This is of particular interest for studying anisotropic superconductors at low temperatures which are expected to show a variety of phenomena related to vortex physics. We successfully tested the apparatus on a 16 mg sample of superconducting niobium ($T_c \simeq$ 9 K). Since the thermometers are calibrated up to room temperature, the same setup can be used to perform measurements in the temperature range 2.5 K to 300 K. This work was done in the framework of a diploma thesis.

In the context of the technical part of another diploma thesis an independent and fully automated device for electrical four-point transport measurements was designed and built. Two main specifications guided the development of this device: 1) The possibility to quickly stabilize the temperature of the sample within 0.1 K; 2) The minimization of thermal gradients across the sample holder, in order to keep the difference between the temperature at the sensor site and the effective temperature at the sample site as small as possible. In order to comply with these requirements, a whole experimental setup was put on stream, comprising a He flow cryostat, a temperature controller for the sample holder, a cryosorption pump (with automatic nitrogen refill relay circuit), a digital nano-voltmeter, a dc current source, and a measurement computer with IEEE interface card. A *Labview* program performs the readings and settings for the actual four-point measurements and controls the sequence in the temperature profile entered by the user.

Basically, the temperature stabilization process involves the temperature controllers of both, the cryostat and the sample holder. As the thermal inertia of the cryostat is large, it

takes up to 10 minutes until a new cryostat temperature is stabilized. However, very fast temperature changes of the sample away from the cryostat temperature could be realized by integrating a powerful heating foil on the sample holder. Thermal relaxation tests revealed that temperature steps of 10 K are well stabilized within about 30 s. The accuracy of typical resistance data was found to be ± 10 $\mu\Omega$.

11.3.2 Electrical transport in doped manganites

A number of experiments have provided strong evidence for the existence of small polaronic charge carriers and their hopping conduction in the paramagnetic state of manganites. However, the nature of the charge carriers and the electrical transport mechanism in the low-temperature metallic state have not been resolved. At low temperatures, a dominant T^2 contribution in resistivity is generally observed, and has been ascribed to electron-electron scattering [26]. Jaime *et al.* [27] have recently shown that the resistivity is essentially temperature independent below 20 K and exhibits a strong T^2 dependence above 50 K. In addition, the coefficient of the T^2 term is about 60 times larger than that expected for electron-electron scattering. They thus ruled out the electron-electron scattering as the conduction mechanism and proposed single magnon scattering with a cutoff at long wavelengths. In their scenario [27], they considered a case where the manganese e_g minority (spin-up) band lies slightly above the Fermi level (in the majority spin-down band) with a small energy gap of about 1 meV. This is in contradiction with optical data [28] which show that the manganese e_g minority band is well above the Fermi level. This suggests that the conduction mechanism proposed in ref. [27] is not relevant.

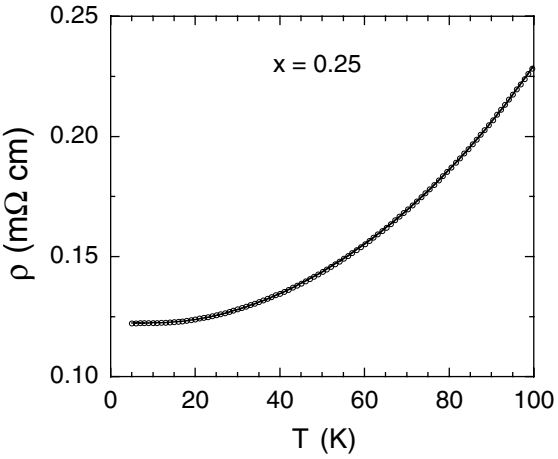

Figure 11.12: *Low temperature resistivity $\rho(T)$ for a high-quality film of $La_{0.75}Ca_{0.25}MnO_3$. The solid line is a fit to the data using Eq. 11.1 with $\hbar\omega_s/k_B$ = 74.5(4) K.*

Recently, Alexandrov and Bratkovsky [4] have proposed a theory for colossal magnetoresistance in doped manganites. Their model predicts that small polaronic transport is the prevalent conduction mechanism even below the ferromagnetic ordering temperature T_C. If their model is indeed relevant, the temperature dependence of the resistivity should agree with polaron metallic conduction. This is indeed the case as demonstrated by us [29]. There are three contributions to the resistivity: the residual resistivity ρ_o, the term $AT^{4.5}$ contributed from 2-magnon scattering [30], and the term $B\omega_s/\sinh^2(\hbar\omega_s/2k_BT)$, which arises from polaron coherent motion involving a relaxation due to a soft optical phonon mode that is strongly coupled to the carriers [29]. Here ω_s is the frequency of a soft optical mode. The low-temperature resistivity is then given by [29, 31]

$$\rho(T) = \rho_o + AT^{4.5} + B\omega_s/\sinh^2(\hbar\omega_s/2k_BT). \qquad (11.1)$$

Fig. 11.12 shows $\rho(T)$ data for a high-quality epitaxial thin film of $La_{0.75}Ca_{0.25}MnO_3$. The data can be well fitted by Eq. 11.1 with $\hbar\omega_s/k_B = 74.5(4)$ K. If we allow the power in the second term of Eq. 11.1 to be a fitting parameter, the best fit gives a power of 4.2(4) [32], very close to 4.5 expected from 2-magnon scattering [30]. Furthermore, the coefficient A is in quantitative agreement with the prediction of 2-magnon scattering [32]. This provides the first bulk experimental evidence of half-metallic ferromagnetism in doped manganites [32].

11.3.3 Phase transition of the vortex lattice in cuprates

It is well known from thermal experiments that the vortex-lattice melting-transition in $YBa_2Cu_3O_{7-\delta}$ for magnetic fields parallel to the crystallographic c-axis is a first-order phase transition [25, 33, 34, 35]. The measured latent heats of melting, $L = T\Delta S$, are in very good agreement with theoretical predictions based on an anisotropic London model [36, 37]. When the applied magnetic field H is tilted away from c, one expects a certain scaling behavior of the melting fields $H_m(T)$ and of the associated discontinuities in entropy, ΔS.

However, it has been concluded from resistivity data in a perfect $H//ab$ geometry that deviations from the standard anisotropic scaling behavior [36, 37] should occur within 0.3 degrees around $H//ab$ [38]. Within this narrow range of angles, we may expect that the vortex physics is influenced by the layered crystal structure of the material, and a state with intrinsic vortex pinning should develop. Early theoretical work has predicted the occurrence of a second-order phase transition of the $H//ab$ Josephson-vortex lattice to a corresponding fluid state [39]. The thermodynamics of this state is experimentally unexplored. Our previous work on the angular dependence of ΔS [25, 33] did not reach sufficient resolution to explore a perfect $H//ab$ geometry. We have very much improved the accuracy, so we can test whether the thermodynamics of the vortex matter near $H//ab$ deviates from continuum-theory expectations or not.

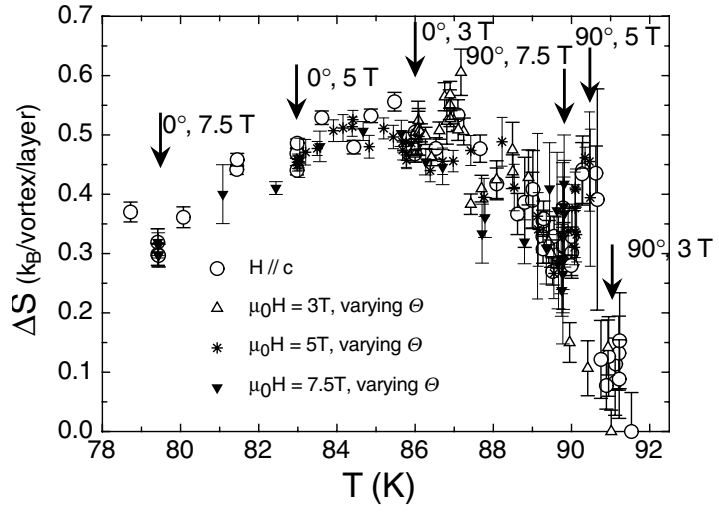

Figure 11.13: *Entropies of vortex-lattice melting in $YBa_2Cu_3O_{7-\delta}$ from 250 specific-heat experiments for varying external magnetic field H and angle Θ between H and the c-axis of the crystal. In agreement with continuum theory, all $\Delta S(T)$ data collapse onto one single curve.*

To do this, we have carefully investigated the angular dependence of the thermodynamic quantities $H_m(T)$ and ΔS of an untwined $YBa_2Cu_3O_{7-\delta}$ single crystal ($T_c = 92.5$ K) using our new high-resolution calorimeter with an angular resolution of 0.01 degrees. We have

performed a series of 250 heat-capacity measurements for a varying $H//c$, and for a fixed $\mu_0 H = 3$ T, 5 T and 7.5 T and varying angle between H and c, respectively (see Fig. 11.13). According to conventional continuum theory, the melting entropies ΔS for $H//ab$ should coincide with the respective data obtained at the same temperature in a $H//c$ geometry. For instance, ΔS for $H//ab$ in $\mu_0 H = 7.5$ T at $T = 89.8$ K should be the same as ΔS for $H//c$ in $\mu_0 H = 0.86$ T for $H//c$ at the same temperature. Within the accuracy of our apparatus, ΔS behaves as predicted by an anisotropic London theory, also for $H//ab$. There is still a measurable latent heat, at exactly the temperature calculated from an anisotropic continuum theory. We do not see any change in the thermodynamics of the vortex system for $H//ab$ in the investigated crystal.

Very recent theoretical [40] and experimental [41] work indicates, however, that significant deviations from continuum theory can occur only in cuprate superconductors with a electronic anisotropy larger than in optimally doped $YBa_2Cu_3O_{7-\delta}$. Suitable candidates for similar experiments are therefore oxygen depleted $YBa_2Cu_3O_{7-\delta}$ and $Bi_2Sr_2CaCu_2O_8$.

11.4 Spectroscopic studies of cuprates (not related to isotope effects)

11.4.1 NMR and NQR studies

In a collaboration with Dr. J. Karpinski (ETHZ) the influence of Sr for Ba substitution on the structure and charge distribution in $YBa_2Cu_4O_8$ was studied by NQR and compared to an extensive bond-valence sum (BVS) investigation [42]. The NQR frequency ν_Q of the plane copper is very sensitive to changes in the density of hole charge carriers n in the CuO_2 planes. NQR experiments for $YBa_2Cu_3O_{7-x}$ and $La_{2-x}Sr_xCuO_4$ show that ν_Q of the plane copper nuclei shifts towards higher values with increasing hole charge carrier concentration in the planes. In the $YBa_2Cu_3O_{7-x}$ family ν_Q changes at 100 K from 23.18 MHz in underdoped $YBa_2Cu_3O_6$ to 31.53 MHz in $YBa_2Cu_3O_7$. In the $La_{2-x}Sr_xCuO_4$ system, ν_Q increases linearly with Sr doping from 33 MHz for x=0 to 36.2 MHz for x=0.15. Assuming that each Sr ion delivers one hole charge carrier into the CuO_2 plane one gets a frequency change of $d\nu_Q/dn$ = 21 MHz/hole. This result is used to estimate the increase of n in the CuO_2 planes of $YBa_{2-x}Sr_xCu_4O_8$ when Ba is substituted by isovalent Sr. The measurements of ν_Q of plane copper in $YBa_{2-x}Sr_xCu_4O_8$ show an increase by 330 kHz for $x = 0.3$ and by 610 kHz for x = 0.6 as compared to the pure $x = 0$ material. The increase in ν_Q is approximately linear in x, and thus one can conclude that the plane hole charge carrier concentration increases by 0.016 hole/Cu for $x = 0.3$ and 0.029 hole/Cu for $x = 0.6$. Since Sr and Ba are isovalent, this increase has to come from a charge redistribution in the structure. With x increasing, ν_Q of chain copper decreases for almost the same value as ν_Q of plane copper increases suggesting a chain to plane hole transfer. These results support BVS calculations which show a general increase of hole concentration and, in addition, a clear indication of redistribution of holes between copper and oxygen in the CuO_2 planes. The estimated values of the charge transfer differ slightly between BVS and NQR results. This is understandable in view of the crudeness of these two empirical approaches, which neglect other effects like volume change and strain caused by substitutions.

In a similar copper NQR study of $YBa_2Cu_4O_8$ the influence on structure and charge distribution by substituting Y with isovalent RE ions was investigated. A clear trend was observed showing an increase in NQR frequencies for plane as well as chain copper sites with increasing ionic radii of RE ions in the sequence Er, Ho, Y, Dy, Gd, Sm, Nd. These findings can be explained by a change in the chain to plane hole transfer, combined with an appreciable variation of lattice parameters, and have to be compared with the results obtained from a detailed BVS investigation.

11.4.2 μSR studies of ruthenocuprates

There have been a number of recent reports of the coexistence of superconductivity and long-range magnetic order in the new class of hybrid ruthenocuprates $RuSr_2LnCu_2O_8$ (Ru-1212) and $RuSr_2(Ln_{1+x}Ce_{1-x})Cu_2O_{10}$ (Ru-1222) (Ln= Sm, Eu, and Gd) [43, 44]. These compounds have a layered structure with alternating CuO_2 and RuO_2 layers. It seems that superconductivity is developed in CuO_2 layers like in high-T_c cuprates and magnetism is due to the RuO_2 planes. Till now most of the reports have focused on a Ru-1212 phase, where the magnetic transition is observed at T_m=133 K and the onset temperature of superconductivity is T_c=35 K. Several experiments were performed to confirm the coexistence of superconductivity and magnetism on a microscopic scale. In particular, Bernhard *et al.* [44] using zero-field (ZF) muon-spin rotation (μSR) technique found that the magnetic order is uniform and homogeneous on a microscopic level.

We decided to focus our attention on a Ru-1222 phase $RuSr_2(Ln_{1.4}Ce_{0.6})Cu_2O_{10}$ (Ln=Eu or Gd), which is actually the first ruthenocuprate where the coexistence of superconductivity and magnetism was found [43]. Recently the specific heat jump at T_c was observed in these samples confirming bulk superconductivity [45]. However, it remains to be demonstrated that the magnetism also has bulk character in order to infer the microscopic coexistence of magnetism and superconductivity. To answer this question we studied $RuSr_2(Ln_{1.4}Ce_{0.6})Cu_2O_{10}$ (Ln=Eu or Gd) using ZF-μSR. Magnetization measurements showed that these samples were superconducting below T_c=40 K and the magnetic transition occurs at T_m=80 K.

The μSR experiments were performed at the Paul Scherrer Institute (PSI), using essentially 100% spin-polarized positive "surface muons". At low temperatures in all studied samples we observed damped oscillations due to muon-spin precession in local magnetic fields. A clear oscillation observed in the ZF-μSR spectra implies that muons sense a well defined internal magnetic field.

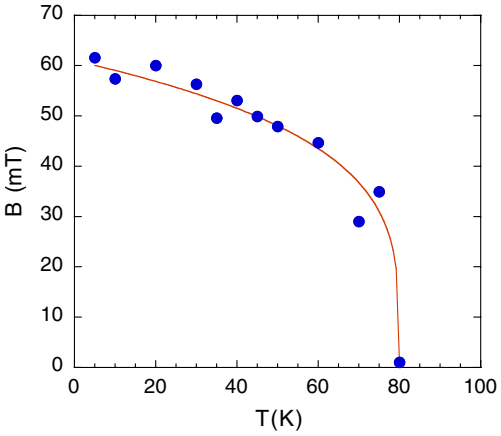

Figure 11.14: *Temperature dependence of the internal magnetic field at the muon site in* $RuSr_2(Eu_{1.4}Ce_{0.6})Cu_2O_{10}$. *The solid line represents a fit with the power law* $B(T) = B(0)(1 - T/T_m)^n$.

Figure 11.14 shows the temperature dependence of the internal magnetic field at the muon site for a $RuSr_2(Eu_{1.4}Ce_{0.6})Cu_2O_{10}$ sample. From the magnitude of the oscillatory component we deduce that the entire sample volume is magnetically ordered. Our ZF-μSR experiments thus provide conclusive evidence of magnetic order in the superconducting Ru-1222 compounds. The magnetism is uniform and homogeneous in the entire sample volume. Therefore there is a microscopic coexistence of superconductivity and magnetism in Ru-1222 compounds.

11.4.3 EPR studies of cuprates

The investigation of high-T_c superconductors has, from a magnetic resonance point of view, till recently been dominated by NMR. The observation of EPR is of great interest, because the time-domain of observation of EPR is two to three orders of magnitude shorter than that of NMR. However, the application of EPR to high-T_c cuprates was restricted owing to the absence of intrinsic EPR signals in these compounds. The reason of the EPR silence in the cuprates is due to the extremely large linewidth. Another approach in the application of EPR to high-T_c superconductors is to dope these compounds with small amounts of paramagnetic ions which are used to probe the intrinsic behavior. One of the best candidates is Mn, which in the 2+ valent state gives a well defined signal and substitutes for the Cu^{2+} in the CuO_2 plane. Recently, Kochelaev *et al.* [46] have intensively studied the EPR of Mn^{2+} doped $La_{2-x}Sr_xCuO_4$. They found that the Mn ions are strongly coupled to the collective motion of the Cu spins (the so called bottleneck regime). The bottleneck regime allows to obtain substantial information on the dynamics of the copper electron spins in the CuO_2 plane [46].

We decided to take advantage of the Mn^{2+} doped $La_{2-x}Sr_xCuO_4$ to probe the copper spin relaxation via the bottleneck effect. Figure 11.15 shows the temperature dependence of the linewidth for samples with different Sr concentration. In all studied samples the linewidth

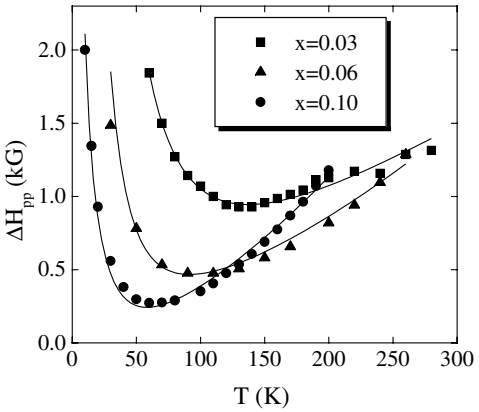

Figure 11.15: *Temperature dependence of the EPR linewidth ΔH_{pp} for $La_{2-x}Sr_xCu_{0.98}Mn_{0.02}O_4$ samples with various concentration x. The solid lines represent the best fit using the theoretical model described in the text.*

decreases with decreasing temperature, passes through a minimum at a temperature T_{min} and increases again on further cooling. The low temperature upturn is more pronounced in underdoped samples and decreases with increasing doping and in addition T_{min} systematically shifts to lower temperatures.

In order to explain the observed temperature dependence of the linewidth, a new theoretical model is proposed that relates the EPR linewidth with the tilting and tunneling modes of the oxygen octahedra around the copper. This model leads to a Hamiltonian in which the Q_4^i and Q_5^i modes are coupled linearly to Dzyaloshinsky-type spin terms [47]:

$$H_{\sigma L} = \frac{J\Lambda}{8a} \sum_{<ij>} \left[\left(\sigma_y^i \sigma_z^j - \sigma_z^i \sigma_y^j\right) \left(Q_4^i - Q_4^j\right) + \left(\sigma_x^i \sigma_z^j - \sigma_z^i \sigma_x^j\right) \left(Q_5^i - Q_5^j\right) \right], \quad (11.2)$$

$$\Lambda = \frac{3\lambda G}{\Delta^2}.$$

Here Q_4^i and Q_5^i are the normal coordinates of the oxygen octahedron CuO_6, which describe its distortions due to the tunneling motion of the apical oxygen between the four potential minima without the rigid rotation of the octahedra as a whole. The constants λ and G correspond to the spin-orbit and orbit-lattice coupling, Δ is the crystal field splitting between the ground and excited orbital energy levels, $< ij >$ means the sum over neighboring Cu sites in the $x - y$ plane, and a is the lattice constant.

Using this Hamiltonian we calculated the temperature dependence of the EPR linewidth and compared it with the experimental data [48]. The solid lines in Fig. 11.15 represent the best fit curves to the theoretical model. One can see that there is a good agreement between theory and experiment. Furthermore, this novel theoretical approach allows an estimation of the intrinsic EPR relaxation time, and provides an explanation for the long-standing problem of EPR silence in high-T_c superconductors. Our estimations show that the intrinsic EPR linewidth from copper spins in these compounds would be of the order of 10^4 G. This value is too large for observing an EPR signal at the usual frequencies.

11.5 Experiments with low-energy muons

As described in the Annual Report 1999/2000, the recent development of a low-energy (LE) muon beam at the Paul Scherrer Institute (PSI) [49, 50] offers completely new possibilities in μSR research in condensed matter physics. These slow muons of tunable energy can be implanted at very small and controllable depth (with nanometer resolution) below the surface of a sample. The spectrum of applications of LE-μSR is unique, including magnetic and superconducting thin films, multilayer systems and structured materials, quasi two-dimensional magnetic systems, and new materials which can only be prepared in thin film form.

Over the last five years the LE-μSR technique was developed by researchers from PSI (E. Morenzoni, project leader) and from the Universities of Birmingham, Braunschweig, Konstanz, and Zurich. In the last year the LE-μSR apparatus was considerably modified to improve its performance. In order to extend the range of possible samples to be investigated by this technique, a new ultra-high vacuum cryostat was built, that allows to perform experiments from 2.4 K up to room temperature. In addition, the magnetic field of the external solenoid was increased to 0.3 Tesla. With the goal to use solid neon as a moderation material in the future, which would increase the intensity of low energy muons by at least 50%, an experimental program was started to improve the cryostat required for the moderation of the low-energy muons. Furthermore, PSI has decided to build a new dedicated surface muon beam line. All these improvements will increase the muon intensity by a factor of 10, making LE-μSR experiments much more efficient in the near future.

References

[1] A.P. Ramirez, J. Phys.:Condens. Matter, **9**, 8171 (1997).

[2] A.J. Millis, P.B. Littlewood, and B.I. Shraiman, Phys. Rev. Lett. **74**, 5144 (1995).

[3] A. Moreo, S. Yunoki, and E. Dagotto, Science **283**, 2034 (1998).

[4] A.S. Alexandrov, A.M. Bratkovsky, Phys. Rev. Lett. **82**, 141 (1999).

[5] G.M. Zhao *et al.*, Phys. Rev. B **63**, R60402 (2001).

[6] A.S. Alexandrov *et al.*, cond-mat/0011436 (submitted to Phys. Rev. Lett.).

[7] G.M. Zhao *et al.*, Phys. Rev. B **62**, R11949 (2000).

[8] F. Raffa, *et al.*, Phys. Rev. Lett. bf 81, 5912 (1998).

[9] G.V.M. Williams, *et al.*, Phys. Rev. Lett. bf 80, 377 (1998).

[10] B. Büchner *et al.*, Phys. Rev. Lett. **73**, 1841 (1994).

[11] J.M. Tranquada, *et al.*, Nature **375**, 56 (1995).

[12] H.A. Mook, *et al.*, Nature (London) **395**, 580 (1998).

[13] V.J. Emery, S.A. Kievelson, and O. Zachar, Phys. Rev. B **56**, 6120 (1997).

[14] A. Lanzara, *et al.* , J. Phys.:Condens. Matter **11**, L541 (1999).

[15] A.W. Hunt, P.M. Singer, K.R. Thurber, and T. Imai, Phys. Rev. Lett. **82**, 4300 (1999).

[16] R. Werner, M.Hücker and B. Büchner, Phys. Rev. B **62**, 3704 (2000).

[17] N.J. Curro, *et al.*, Phys. Rev. Lett. bf 85, 642 (2000) and M.-H. Julien, *et al.* (cond-mat/0010362).

[18] A. S. Alexandrov and N.F. Mott, Int. J. Mod. Phys. **8**, 2075 (1994).

[19] K.A. Müller, Physica C **341-348**, 11 (2000).

[20] G.M. Zhao *et al.*, Nature **385**, 236 (1997).

[21] G.M. Zhao et al., J. Phys.: Codens. Matter **10**, 9055 (1998).

[22] J. Hofer *et al.*, Phys. Rev. Lett. **84**, 4192 (2000).

[23] P. Zimmerman *et al.*, Phys. Rev. B **52**, 541 (1995).

[24] A. Schilling and O. Jeandupeux, Phys. Rev. B **52**, 9714 (1995).

[25] A. Schilling *et al.*, Nature **382**, 791 (1996).

[26] A. Urushibara *et al.*, Phys. Rev. B **51**, 14103 (1995).

[27] M. Jaime *et al.*, Phys. Rev. B **58**, R5901 (1998).

[28] A. Machida, Y. Moritomo, and A. Nakamura, Phys. Rev. B **58**, R4281 (1998).

[29] G.M. Zhao *et al.*, Phys. Rev. Lett. **84**, 6086 (2000).

[30] K. Kubo and N.A. Ohata, J. Phys. Soc. Jpn. **33**, 21 (1972).

[31] G.M. Zhao, H. Keller, and W. Prellier, J. Phys.: Condens. Matter **12**, L361 (2000).

[32] G.M. Zhao *et al.*, Phys. Rev. B (in press).

[33] A. Schilling *et al.*, Phys. Rev. Lett. **76**, 4833 (1997).

[34] M. Willemin *et al.*, Phys. Rev. Lett. **81**, 4236 (1998).

[35] A. Schilling *et al.*, Phys. Rev. B. **61**, 3592 (2000).

[36] G. Blatter *et al.*, Phys. Rev. Lett. **68**, 875 (1992).

[37] M.W. Dodgson *et al.*, Phys. Rev. B. **57**, 14498 (1998).

[38] W.K. Kwok *et al.*, Phys. Rev. Lett. **67**, 390 (1991).

[39] X. Hu and M. Tachiki, Phys. Rev. Lett. **80**, 4044 (1998).

[40] X. Hu and M. Tachiki, Phys. Rev. Lett. **85**, 2577 (2000).

[41] S.N. Gordeev *et al.*, Phys. Rev. Lett. **85**, 2577 (2000).

[42] J. Karpinski *et al.*, submitted to Phys. Rev. B.

[43] I. Felner *et al.*, Phys. Rev. B **55**, R3374 (1997).

[44] C. Bernhard *et al.*, Phys. Rev. B **59**, 14099 (1999).

[45] X.H. Chen *et al.*, J. Phys.: Condens. Matter **12**, 10561 (2000).

[46] B.I. Kochelaev *et al.*, Phys. Rev. B **49**, 13106 (1994).

[47] B.I. Kochelaev, J. Supercond., **12**, 53 (1999).

[48] A. Shengelaya *et al.*, to be published in Phys. Rev. B

[49] E. Morenzoni *et al.*, J. Appl. Phys. **81**, 3340 (1997).

[50] E. Morenzoni, *Physics and applications of low energy muons*, in Muon Science, S.L. Lee *et al.* Eds., IOP Publishing (1999).